








Quiescent Low-mass Galaxies Observed by JWST in the Epoch of Reionization

Viola Gelli^{1,2} , Stefania Salvadori^{1,2} , Andrea Ferrara³ , Andrea Pallottini³ , and Stefano Carniani³ 

¹Dipartimento di Fisica e Astronomia, Università degli Studi di Firenze, via G. Sansone 1, I-50019, Sesto Fiorentino, Italy; viola.gelli@unifi.it

²INAF/Osservatorio Astrofisico di Arcetri, Largo E. Fermi 5, I-50125, Firenze, Italy

³Scuola Normale Superiore, Piazza dei Cavalieri 7, I-56126, Pisa, Italy

Received 2023 March 24; revised 2023 July 19; accepted 2023 August 7; published 2023 August 25

Abstract

The surprising JWST discovery of a quiescent, low-mass ($M_* = 10^{8.7} M_\odot$) galaxy at redshift $z = 7.3$ (JADES-GS-z7-01-QU) represents a unique opportunity to study the imprint of feedback processes on early galaxy evolution. We build a sample of 130 low-mass ($M_* \lesssim 10^{9.5} M_\odot$) galaxies from the SERRA cosmological zoom-in simulations, which show a feedback-regulated, bursty star formation history (SFH). The fraction of time spent in an active phase increases with the stellar mass from $f_{\text{duty}} \approx 0.6$ at $M_* \approx 10^{7.5} M_\odot$ to ≈ 0.99 at $M_* \geq 10^9 M_\odot$, and it is in agreement with the value $f_{\text{duty}} \approx 0.75$ estimated for JADES-GS-z7-01-QU. On average, 30% of the galaxies are quiescent in the range $6 < z < 8.4$; they become the dominant population at $M_* \lesssim 10^{8.3} M_\odot$. However, none of these quiescent systems matches the spectral energy distribution of JADES-GS-z7-01-QU, unless their SFH is artificially truncated a few Myr after the main star formation peak. As supernova feedback can only act on a longer timescale ($\gtrsim 30$ Myr), this implies that the observed abrupt quenching must be caused by a faster physical mechanism, such as radiation-driven winds from young massive stars and/or an active galactic nucleus.

Unified Astronomy Thesaurus concepts: [High-redshift galaxies \(734\)](#); [Galaxy evolution \(594\)](#); [Galaxy formation \(595\)](#); [Cosmology \(343\)](#)

1. Introduction

The growth of galaxies is regulated by the conversion of cold gas into stars and is affected by different feedback processes (Ciardi & Ferrara 2005), which can lead to the temporary or definitive quenching of the star formation activity. Internal feedback mechanisms include radiative feedback, which can destroy H_2 molecules preventing gas cooling (e.g., Johnson et al. 2007; Krumholz et al. 2009), and mechanical feedback from massive stars/supernovae (SN) or active galactic nuclei (AGNs), which can partially or completely remove the gas reservoir (e.g., Mac Low & Ferrara 1999; Croton et al. 2016; Carnall et al. 2023).

The evolution of low-mass galaxies, which we define here as those with stellar mass $M_* \leq 10^{9.5} M_\odot$, is dramatically affected, regulated, and—in some cases—even halted by these physical mechanisms because of their shallow potential well (e.g., Ferrara & Tolstoy 2000; Salvadori et al. 2008; Wise et al. 2012; Collins & Read 2022). Furthermore, these systems can also be impacted by more global feedback mechanisms, such as reionization, preventing the accretion of fresh gas into the less-massive systems (e.g., Gnedin 2000; Dijkstra et al. 2004; Sobacchi & Mesinger 2013; Pereira-Wilson et al. 2023), and environmental effects, such as ram pressure stripping, which can remove the interstellar medium from satellite galaxies (e.g., Mayer et al. 2006; Emerick et al. 2016; Boselli et al. 2022). Thus, low-mass galaxies are the ideal laboratory to investigate feedback processes.

In the early Universe, low-mass galaxies are very common. Thanks to JWST we can now study them and investigate the role of the various feedback processes in their evolution. Looser et al. (2023) recently reported the discovery of a quiescent low-mass galaxy at redshift $z = 7.3$ (see also Strait et al. 2023 for another very low-mass quiescent system at $z = 5.2$) from the JADES

program, JADES-GS-z7-01-QU. Following this work, we define as *quiescent* those galaxies with no (or negligible) star formation activity at the epoch of observation.⁴ According to Looser et al. (2023), the spectral energy distribution (SED) of JADES-GS-z7-01-QU is consistent with a metal-poor $M_* \approx 5 \times 10^8 M_\odot$ stellar population formed in a short and intense burst of star formation followed by rapid quenching (star formation rate (SFR) $< 10^{-2.5} M_\odot \text{ yr}^{-1}$), about 10–20 Myr before the epoch of observation. Given the rapidity of the transition from a star-forming to a quiescent state for JADES-GS-z7-01-QU, its quenching is expected to have been driven by a fast process. A reasonable explanation may therefore be associated with the injection of mechanical energy through outflows by either star formation or AGN.

In this Letter, we aim to interpret these new findings and address the following questions: What is the duty cycle of high-redshift low-mass galaxies? When and why do low-mass galaxies become quiescent? What are the key physical mechanisms causing their quenching?

2. Simulated Low-mass Galaxies

To answer the above questions, we use the SERRA (Pallottini et al. 2022) suite of high-resolution cosmological zoom-in simulations that follow the evolution of typical Lyman break galaxies during the Epoch of Reionization. The simulations evolve from $z = 100$, where initial conditions are generated with MUSIC (Hahn & Abel 2011), in a cosmological volume of $(20 \text{ Mpc}/h)^3$ by assuming a Planck Collaboration et al. (2014) cosmology.⁵ A customized version of the Adaptive Mesh

⁴ Note that in the literature, quiescent galaxies are sometimes differently defined as those below the main sequence (Houston et al. 2023), or quenched for > 500 Myr (Pérez-González et al. 2023).

⁵ Throughout the paper we assume a Λ CDM model with vacuum, matter, and baryon densities in units of the critical density $\Omega_\Lambda = 0.692$, $\Omega_m = 0.308$, and $\Omega_b = 0.0481$, Hubble constant $H_0 = 67.8 \text{ km s}^{-1} \text{ Mpc}^{-1}$, spectral index $n = 0.967$, and $\sigma_8 = 0.826$.

Refinement code RAMSES (Teyssier 2002) is used for the evolution of dark matter (DM), stars, and gas, reaching a baryon mass resolution of $1.2 \times 10^4 M_\odot$ and spatial resolution of $\simeq 20$ pc in the zoom-in regions, i.e., about the mass and size of molecular clouds.

On-the-fly radiative transfer is included through RAMSES-RT (Rosdahl et al. 2013), and a nonequilibrium chemical network generated with KROME (Grassi et al. 2014) is used for regulating the interaction of the gas with photons (Pallottini et al. 2017a). Stars form according to a Schmidt–Kennicutt relation (Kennicutt 1998) depending on the molecular-hydrogen gas density and assuming a Kroupa (2001) initial mass function for the stellar particles. Stellar feedback modeling includes SNe explosions, winds, and radiation pressure (Pallottini et al. 2017b). The energy inputs and chemical yields, depending on the stellar age and metallicity, are computed through STARBURST99 (Leitherer et al. 1999) using PADOVA stellar tracks (Bertelli et al. 1994), covering a metallicity range of $Z_*/Z_\odot = 0.02\text{--}1.0$. Since the resolution does not allow us to follow the evolution of the first stars and mini-haloes, their effect on the interstellar medium (ISM) is reproduced by setting the initial gas metallicity to a floor value of $Z_{\text{floor}} = 10^{-3} Z_\odot$ (Wise et al. 2012; Pallottini et al. 2014).

The emission of the galaxies is modeled using STARBURST99 for the stellar and nebular continuum (see also Gelli et al. 2021). We use CLOUDY (Ferland et al. 2017) to compute nebular line emission (considering the main ones typically contributing to the rest-frame UV-optical spectrum, i.e., H α , H β , H γ , [O II] $\lambda\lambda$ 3726,3729, [O III] $\lambda\lambda$ 4959,5007, and C III] 1909), accounting for the ISM density, metallicity, internal structure, and radiation field (e.g., Vallini et al. 2018; Kohandel et al. 2019; Pallottini et al. 2019). Finally, we take into account the presence of dust, which attenuates the intrinsic galaxy spectrum (i.e., Gelli et al. 2021), adopting a dust-to-metal ratio $f_d = 0.08$ and assuming a Milky Way-like dust composition and grain size distribution⁶ (Weingartner & Draine 2001).

We analyze multiple snapshots of different SERRA runs in the range $6 < z < 8.4$. We follow the stellar-density method implemented in Gelli et al. (2020) to select low-mass galaxies with $M_* \lesssim 10^{9.5} M_\odot$. The final sample has 130 galaxies.

As an example, in Figure 1 we show stellar and gas density maps from one of the simulations at $z = 6$. The displayed volume (10^6 kpc³) contains six galaxies. In the two insets, we zoom on typical low-mass systems: an actively star-forming ($\log M_*/M_\odot = 8.97$), and a quiescent system with no ongoing star formation ($\log M_*/M_\odot = 7.96$). The former shows an extended (~ 500 pc in radius) stellar distribution, and a gas proto-disk structure, typical of more massive galaxies. The quiescent galaxy is instead smaller, both in terms of stellar mass and size, with all of its stars concentrated in the inner $\lesssim 200$ pc, and almost completely devoid of gas.

3. Nature of Quiescent Systems

In Figure 2 we show the star formation histories (SFHs) in terms of age of the Universe t_H for some SERRA low-mass galaxies up to different observation redshifts. The SFHs have

⁶ This choice is driven by Atacama Large Millimetre/submillimeter Array measurements of high- z galaxies (Bouwens et al. 2022) that support an Milky Way-like dust (Ferrara et al. 2022) and low dust-to-metal ratios (Laporte et al. 2017; Behrens et al. 2018). However, the use of different extinction curves (e.g., SMC, LMC) does not lead to significant changes in the emission of low-mass galaxies.

an intermittent nature made of bursts followed by star formation drops or even halts. Such behavior results from stellar feedback, efficiently decreasing or even suppressing star formation in low-mass galaxies. Note that all galaxies with final mass $M_* \lesssim 10^9 M_\odot$ have experienced quiescent SF phases, or are still quenched at the final snapshot, which is identified as the redshift of observation. On average, these quenched galaxies represent 30% of the population.

Interestingly, after the SF peak, these low-mass galaxies feature a smooth SFR decrease lasting some tens of Myr until the final quenching. This trend is typical of stellar feedback powered by SNe, as explosions occur with a delay time that increases with a decreasing SN progenitor mass (see Gelli et al. 2020). This behavior is encountered in all low-mass systems, i.e., in both field and satellite galaxies, implying that environmental processes do not drive their evolution.

In the middle panel of Figure 2, we pinpoint the galaxy *Lilium*, which is quiescent at $z = 7.3$ and has the same stellar mass as JADES-GS-z7-01-QU ($10^{8.7} M_\odot$).

Figure 3 shows the galaxy SFR duty cycle, i.e., the ratio between the actively star-forming (SFR > 0) time interval, Δt_{on} , and the time elapsed between the first star formation event, t_{form} , and the observation redshift at t_{obs} :

$$f_{\text{duty}} = \frac{\Delta t_{\text{on}}}{t_{\text{obs}} - t_{\text{form}}}. \quad (1)$$

Galaxies are color-coded with the mass-averaged age of their stellar populations; quiescent systems (Q1–Q4) identified in Figure 2 are specifically indicated.

Galaxies with $M_* < 10^9 M_\odot$ can be either quiescent or active, and the fraction of quiescent systems increases with decreasing stellar mass, becoming the dominating population for $M_* < 10^{8.3} M_\odot$ (see histograms in the upper panel of Figure 3). In this mass range, quiescent galaxies (a) are older (average ages > 100 Myr), and (b) have lower and more scattered duty cycles ($f_{\text{duty}} \approx 0.2\text{--}0.9$) than active galaxies ($f_{\text{duty}} \approx 0.8\text{--}0.99$). For $M_* > 10^9 M_\odot$, instead, all galaxies are active, and they have been forming stars for $\geq 95\%$ of their lifetime.

The average duty cycle of quiescent and active galaxies clearly reflects these trends with stellar mass, slowly increasing from $f_{\text{duty}} \approx 0.6$ for $M_* \approx 10^{7.5} M_\odot$ to ≈ 0.99 for $M_* \geq 10^9 M_\odot$. Noticeably, the quiescent galaxy *Lilium* ($\log M_*/M_\odot = 8.7$) has a duty cycle $f_{\text{duty}} \approx 0.84$, which is consistent with the values obtained for JADES-GS-z7-01-QU using different stellar population synthesis tools by Looser et al. (2023). For instance, when considering the values derived with BAGPIPES in Table 1 therein,⁷ the time from the first star formation event is $t_{\text{obs}} - t_{\text{form}} \approx 40$ Myr, and the time of active star formation is $\Delta t_{\text{on}} \approx 30$ Myr. This implies a duty cycle (see Equation (1)) for JADES-GS-z7-01-QU of $f_{\text{duty}} \approx 0.75$.

4. Comparison with JWST Observations

Lilium was selected among SERRA quiescent galaxies due to its similarity with JADES-GS-z7-01-QU in terms of stellar mass, duty cycle (Figure 3), and the time elapsed between SF quenching and observation redshift ($\Delta t_{\text{quench}} \sim 15$ Myr for *Lilium* versus $\Delta t_{\text{quench}} \sim 10\text{--}40$ Myr for JADES-GS-z7-01-QU). However, the stellar populations of *Lilium* are more

⁷ Note that in Looser et al. (2023) t_{form} is defined as lookback time from the observation, while in this paper it is defined in terms of the age of the Universe.

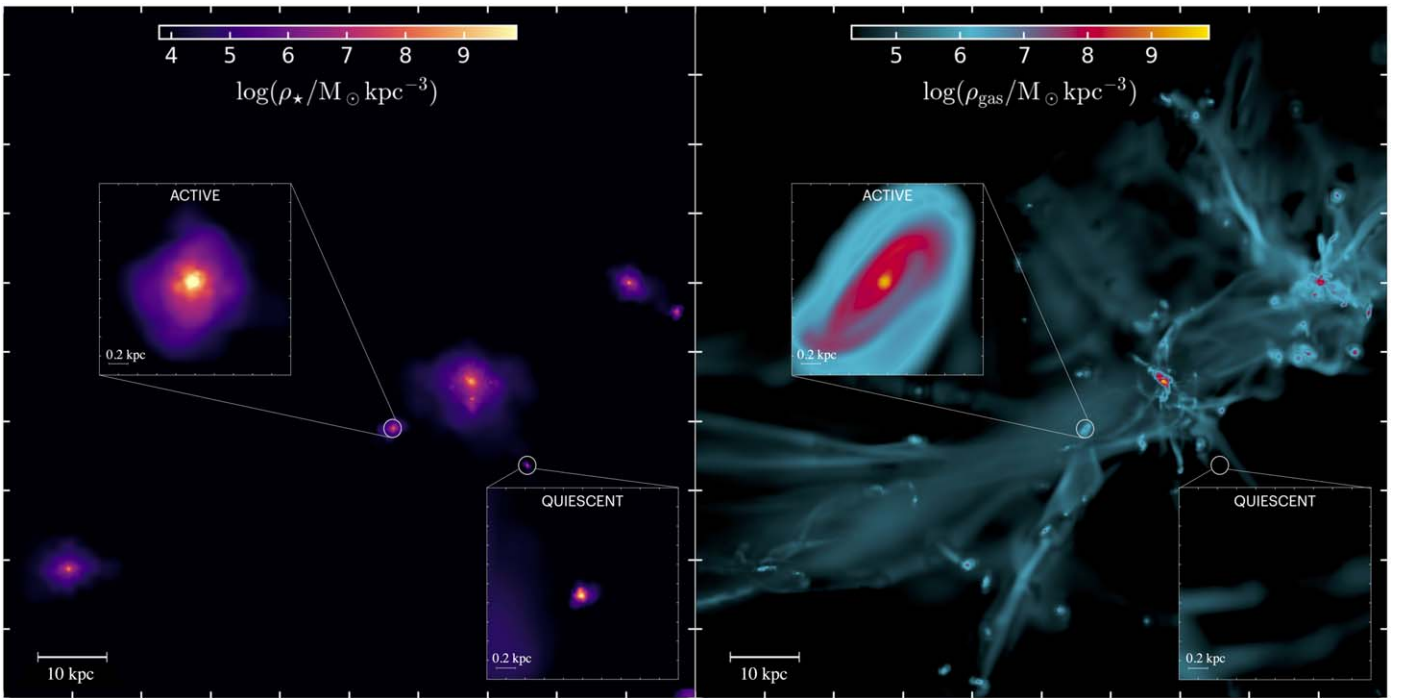


Figure 1. Example of stellar (ρ_* , left) and gas (ρ_{gas} , right) density maps of a system at $z = 6$ within the SERRA simulations. The field of view of $100 \text{ kpc} \times 100 \text{ kpc}$ contains six galaxies. The insets show two zoomed regions, each of size $2 \text{ kpc} \times 2 \text{ kpc}$, centered on a typical quiescent ($\log M_*/M_\odot = 7.96$) and active ($\log M_*/M_\odot = 8.97$) galaxy, as indicated.

metal-rich ($Z_* \approx Z_\odot$) than deduced by Looser et al. (2023) for JADES-GS-z7-01-QU, $Z_* \approx 0.01 Z_\odot$. In spite of these similarities, the SED we predict for *Lilium* (Figure 4, left panel) is too faint to match the one observed in JADES-GS-z7-01-QU. What is the origin of such a discrepancy?

We first check the role of stellar metallicity by imposing that all the stars in *Lilium* have $Z_* \approx 0.01 Z_\odot$. However, the resulting SED only increases by $\lesssim 0.2$ dex (see Figure 4, left panel). The right panel of Figure 4 displays the SFH of *Lilium*. At $z \approx 8.4$, i.e., around 120 Myr before observations, *Lilium* started to form stars at a progressively increasing rate. After ≈ 35 Myr it experienced a short and intense burst of star formation ($\text{SFR} \gtrsim 25 M_\odot \text{ yr}^{-1}$), after which 80% of the final stellar mass was already in place. Then, the SFR was gradually suppressed by SNe, which are the dominating feedback mechanism in our simulations. Indeed, the galaxy continued to form stars at a much lower rate, $\lesssim 2 M_\odot \text{ yr}^{-1}$, for ≈ 50 Myr, i.e., up to $z \approx 7.45$ when it was completely quenched. Therefore, at the redshift of observation, $z = 7.3$, the average stellar age of *Lilium* is ≈ 90 Myr old (see the color bar in Figure 3).

In the same panel, we plot an SFH similar to the one derived by Looser et al. (2023) using BAGPIPES, essentially a top-hat with an $\text{SFR} = 15 M_\odot \text{ yr}^{-1}$ but with the same Δt_{quench} and M_* as *Lilium*. With this SFR, the observed M_* is produced in only ≈ 30 Myr, resulting in a much younger (≈ 30 Myr) stellar population. The other SED-fitting codes⁸ used by Looser et al. (2023), PROSPECTOR (Johnson et al. 2021) and PXF (Cappellari 2017), also draw similar conclusions, resulting in average stellar ages always lower than $\lesssim 50$ Myr. As a consequence, the corresponding experimentally derived SED

reaches fluxes about 10 times higher than *Lilium* (Figure 4, left) and matches JADES-GS-z7-01-QU photometry if a metallicity of $0.01 Z_\odot$ is further assumed.

This result shows that the discrepancy between the SEDs of *Lilium* and JADES-GS-z7-01-QU is largely due to differences in their SFHs, and to a lesser extent, metallicity. The key difference is the fact the SFRs decrease in *Lilium* after the SF peak is too prolonged, resulting in a high fraction of old stars at the time of the observation. This suggests the need for an abrupt quenching right after the SF peak.

To test this hypothesis, we artificially impose that SF in *Lilium* was abruptly halted ~ 5 Myr after the peak, and we renormalize it to get the same M_* value. We then assume to observe the galaxy after $\Delta t_{\text{quench}} = 10\text{--}20$ Myr from the halt, and thus shift the SFHs to match the redshift of the observations, i.e., $z = 7.3$. As a consequence of the overall galaxy lifetime time being shorter, the duty cycle of *Lilium* lowers to ≈ 0.7 . We find that such modified *Lilium* SED now perfectly matches the observed one even by assuming the simulated stellar metallicity, $Z_* \approx Z_\odot$.

5. Discussion

In spite of the fact that *Lilium* is very similar to JADES-GS-z7-01-QU, the simulated SED does not match the observed one. We have shown that this is due to the fact that star formation in JADES-GS-z7-01-QU is quenched on a much shorter timescale than in *Lilium*.

If the quenching has to be produced by SNe, there is an intrinsic timescale on which such feedback acts, which is given by the time over which SNe associated with a given burst explode. This value is $\gtrsim 30$ Myr for a Kroupa initial mass function (see, e.g., Figure 2 in Pallottini et al. 2017a). The quenching cannot, therefore, be significantly shorter than this minimum value, and this is exactly what we see in the SFH of

⁸ The code BEAGLE (Chevallard & Charlot 2016) is also used in Looser et al. (2023). However, since it does not provide a reconstruction of the SFH or the average stellar age, a direct comparison with this model is not possible.

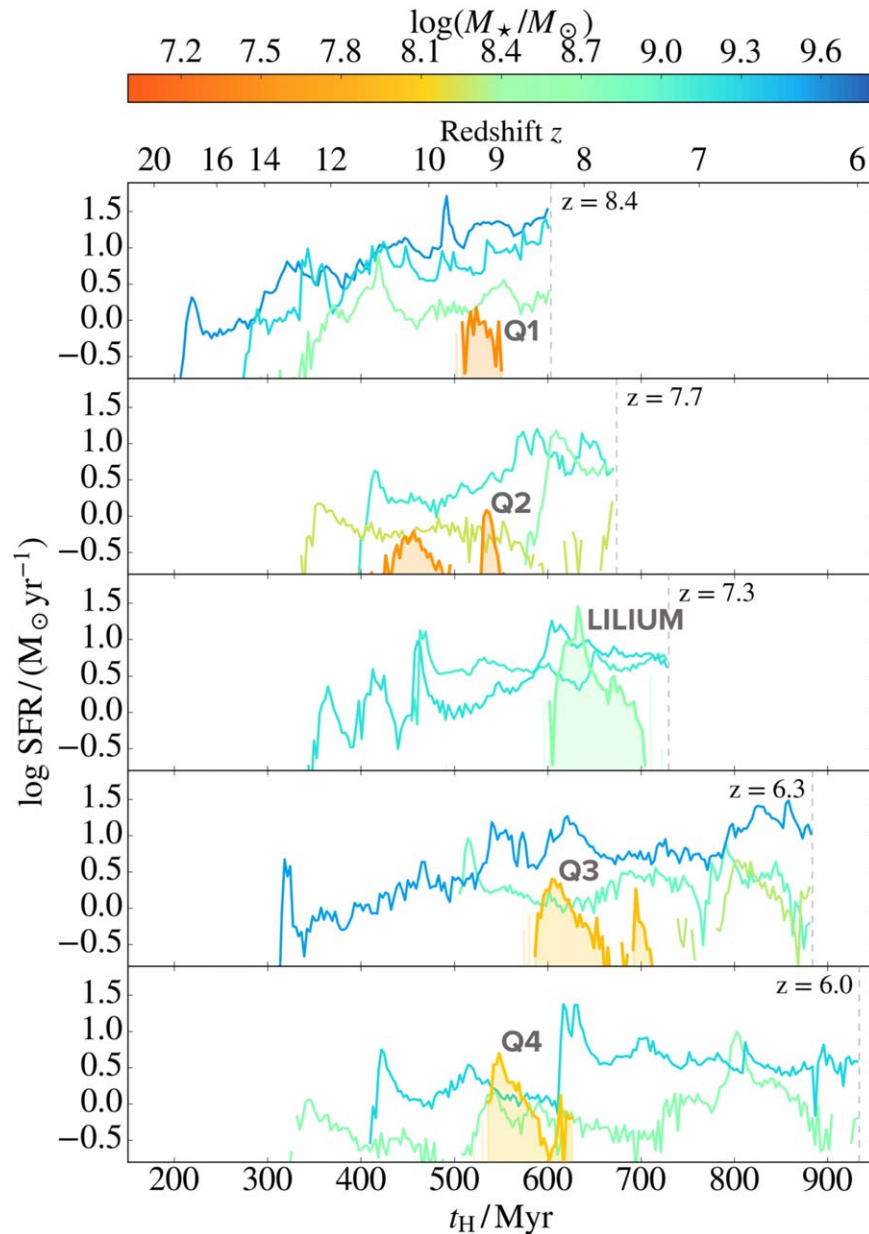


Figure 2. Star formation rate (SFR) as a function of the age of the Universe (t_H) for some SERRA galaxies simulated up to different redshifts, color-coded with the final stellar mass. Filled curves and names denote galaxies that are quiescent at the end of the simulations (30% of the sample).

Lilium and the other quenched low-mass galaxies (Q1, Q2, Q3, and Q4). Basically, the SFR decline under the action of SN feedback is very gradual, resulting in too large a number of stars that are old by the time the galaxy is observed. This is a general problem of SF quenching in low-mass galaxies, which inherently depends on the delay of SN explosions associated with the deaths of progenitors of different masses (e.g., Rosdahl et al. 2017).

We speculate that the decline could be more abrupt if the mechanical energy is instead provided by a hidden AGN and/or radiation pressure from young massive stars (e.g., Carniani et al. 2016; Ferrara et al. 2023; Ziparo et al. 2023). Indeed, we may in general estimate the quenching timescale as $\Delta t_{\text{quench}} = t_{\text{delay}} + t_{\text{ej}}$, where t_{delay} is the delay time associated with the onset of the physical process causing the quenching and t_{ej} is the ejection time required for the outflow to drive the gas out of the galaxy. While for SNe we have $t_{\text{delay}} \gtrsim 30$ Myr,

for radiation-driven feedback there is no such delay, and we can evaluate the overall quenching timescale simply as $\Delta t_{\text{quench}} = t_{\text{ej}}$. Assuming a typical outflow velocity of $v > 200 \text{ km s}^{-1}$ and requiring an expelling of the gas at a distance of $d \approx 500 \text{ pc}$ to quench star formation (given that the effective radius of the galaxy is $\approx 100 \text{ pc}$), we obtain $\Delta t_{\text{quench}} = d/v \lesssim \frac{500 \text{ pc}}{200 \text{ km s}^{-1}} = 2.4 \text{ Myr}$. The gas in the galaxy is expected to be set in motion and removed in such a short time as soon as the galaxy exceeds the Eddington limit. Specifically, this can happen through (i) stellar radiation, when the specific SFR exceeds a threshold value ($> 13 \text{ Gyr}^{-1}$; see Fiore et al. 2023), and (ii) AGN feedback from massive black holes that may be a viable solution for high- z galaxies according to recent results (e.g., Maiolino et al. 2023). We therefore conclude that the SFR decline might be a powerful diagnostic of different feedback types.

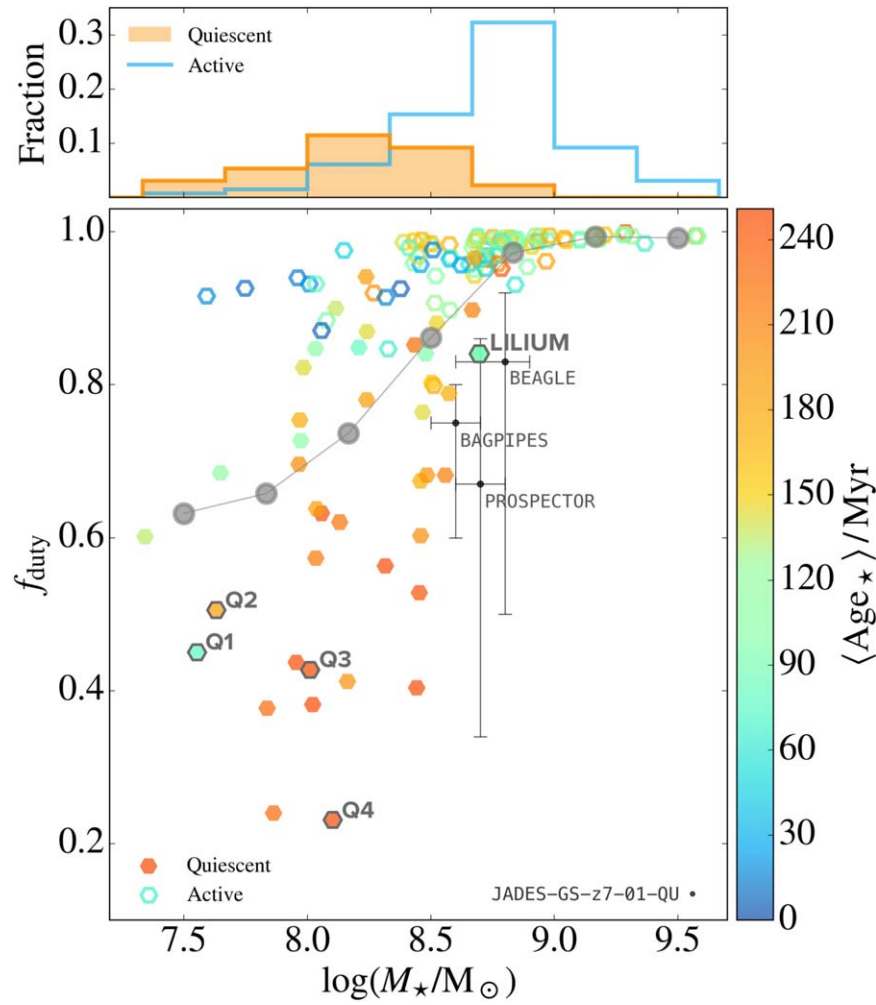


Figure 3. Duty cycle f_{duty} as a function of the stellar mass of quiescent (filled) and active (hollow) galaxies, colored with the average age of the stellar population. The average trend of f_{duty} with the mass is shown through the gray circles. The three points with error bars are the values inferred for JADES-GS-z7-01-QU using different spectral fitting codes (BAGPIPES by Carnall et al. 2018; PROSPECTOR by Johnson et al. 2021; BEAGLE by Chevillard & Charlot 2016) derived from Table 1 of Looser et al. (2023). The histograms in the upper panels show the stellar mass distribution of active and quiescent low-mass galaxies.

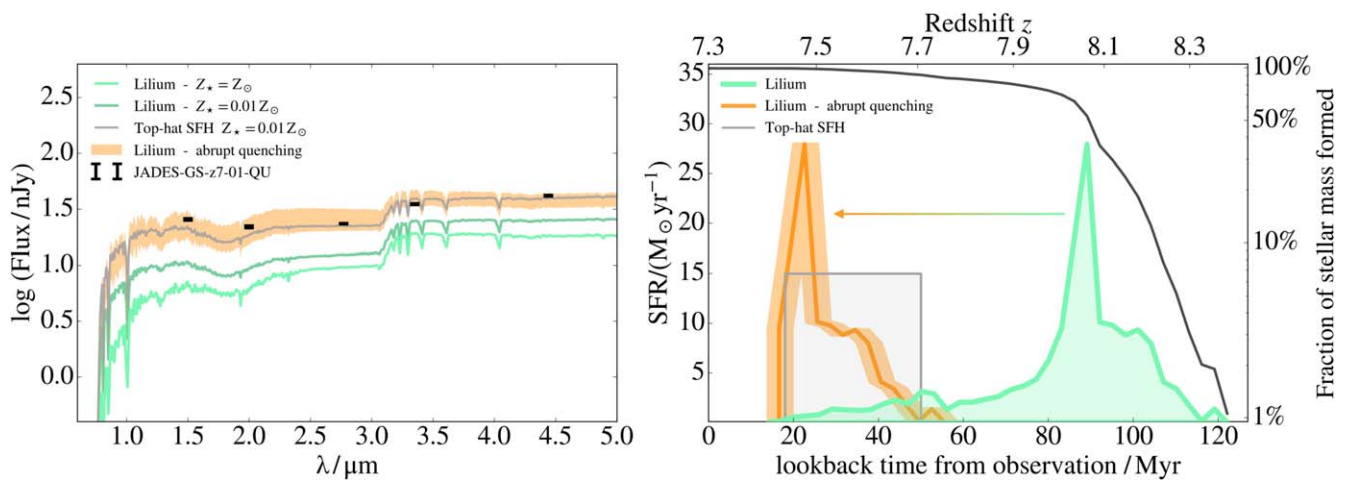


Figure 4. Spectral energy distributions of simulated galaxies at $z = 7.3$ compared with JADES-GS-z7-01-QU (left panel), and corresponding star formation histories (right). Shown in the two figures are the SEDs and SFHs for (a) *Lilium* with two stellar metallicities as indicated (green), (b) an idealized top-hat SFH model with constant SFR (gray), and (c) *Lilium* with a modified SFH featuring an abrupt quenching ≈ 5 Myr after the main peak of star formation and observed after Δt_{quench} varying between 15 and 20 Myr (orange). The black curve in the right panel shows the fraction of stellar mass formed for *Lilium*.

Another puzzle posed by the JADES-GS-z7-01-QU observation is its long latency before the first episode of star formation. This source is observed at $z = 7.3$ and, according to

the SED interpretation, has formed all of its stars in a short (≈ 30 Myr) burst. This sets the start of its star formation activity at $z \approx 7.8$. From the observed stellar mass $M_{\star} = 10^{8.7} M_{\odot}$, and

conservatively assuming that all its baryons were turned into stars, we can set a lower limit to the host halo, $M \gtrsim (\Omega_m/\Omega_b)M_* = 3.2 \times 10^9 M_\odot$. Assuming a standard growth history, this halo should have crossed the critical mass $M \approx 10^8 M_\odot$, marking the separation between mini-halos, in which the SF is easily suppressed, and the star-forming Ly α -cooling halos at $z \gtrsim 11.7$. Thus, in the redshift interval $7.8 < z < 11.7$ (280 Myr), although conditions were in principle favorable to star formation in terms of gas cooling, the galaxy did not form a significant amount of stars. A possibility might be the following: if a galaxy spawns a massive stellar cluster ($M_* \simeq 10^5 M_\odot$) as its first star formation event, its radiation can photodissociate molecular hydrogen and prevent further star formation for up to ~ 300 Myr (see Alyssum; Pallottini et al. 2022).

As JWST will build a sizable sample of quiescent high- z galaxies, we will be able to solve these puzzles and understand the nature of the feedback-regulated evolution of low-mass systems.

Acknowledgments

This project received funding from the ERC Starting Grant NEFERTITI H2020/804240 (PI: Salvadori). A.F., A.P., and S.C. acknowledge the ERC Advanced Grant INTERSTELLAR H2020/740120 (PI: Ferrara). We acknowledge the CINECA award under the ISCRA initiative, for the availability of high performance computing resources and support from Class B project SERRA HP10BPUZ8F (PI: Pallottini) and the computational resources of the Center for High Performance Computing (CHPC) at SNS.

ORCID iDs

Viola Gelli  <https://orcid.org/0000-0001-5487-0392>
 Stefania Salvadori  <https://orcid.org/0000-0001-7298-2478>
 Andrea Ferrara  <https://orcid.org/0000-0002-9400-7312>
 Andrea Pallottini  <https://orcid.org/0000-0002-7129-5761>
 Stefano Carniani  <https://orcid.org/0000-0002-6719-380X>

References

- Behrens, C., Pallottini, A., Ferrara, A., Gallerani, S., & Vallini, L. 2018, *MNRAS*, 477, 552
- Bertelli, G., Bressan, A., Chiosi, C., Fagotto, F., & Nasi, E. 1994, *A&AS*, 106, 275
- Boselli, A., Fossati, M., & Sun, M. 2022, *A&ARv*, 30, 3
- Bouwens, R. J., Smit, R., Schouws, S., et al. 2022, *ApJ*, 931, 160
- Cappellari, M. 2017, *MNRAS*, 466, 798
- Carnall, A. C., McLeod, D. J., McLure, R. J., et al. 2023, *MNRAS*, 520, 3974
- Carnall, A. C., McLure, R. J., Dunlop, J. S., & Davé, R. 2018, *MNRAS*, 480, 4379
- Carniani, S., Marconi, A., Maiolino, R., et al. 2016, *A&A*, 591, A28
- Chevallard, J., & Charlot, S. 2016, *MNRAS*, 462, 1415
- Ciardi, B., & Ferrara, A. 2005, *SSRv*, 116, 625
- Collins, M. L. M., & Read, J. I. 2022, *NatAs*, 6, 647
- Croton, D. J., Stevens, A. R. H., Tonini, C., et al. 2016, *ApJS*, 222, 22
- Dijkstra, M., Haiman, Z., Rees, M. J., & Weinberg, D. H. 2004, *ApJ*, 601, 666
- Emerick, A., Mac Low, M.-M., Grcevich, J., & Gatto, A. 2016, *ApJ*, 826, 148
- Ferland, G. J., Chatzikos, M., Guzmán, F., et al. 2017, *RMxAA*, 53, 385
- Ferrara, A., Pallottini, A., & Dayal, P. 2023, *MNRAS*, 522, 3986
- Ferrara, A., Sommovigo, L., Dayal, P., et al. 2022, *MNRAS*, 512, 58
- Ferrara, A., & Tolstoy, E. 2000, *MNRAS*, 313, 291
- Fiore, F., Ferrara, A., Bischetti, M., Feruglio, C., & Travascio, A. 2023, *ApJL*, 943, L27
- Gelli, V., Salvadori, S., Ferrara, A., Pallottini, A., & Carniani, S. 2021, *ApJL*, 913, L25
- Gelli, V., Salvadori, S., Pallottini, A., & Ferrara, A. 2020, *MNRAS*, 498, 4134
- Gnedin, N. Y. 2000, *ApJ*, 542, 535
- Grassi, T., Bovino, S., Schleicher, D. R. G., et al. 2014, *MNRAS*, 439, 2386
- Hahn, O., & Abel, T. 2011, *MNRAS*, 415, 2101
- Houston, T., Croton, D. J., & Sinha, M. 2023, *MNRAS*, 522, L11
- Johnson, B. D., Leja, J., Conroy, C., & Speagle, J. S. 2021, *ApJS*, 254, 22
- Johnson, J. L., Greif, T. H., & Bromm, V. 2007, *ApJ*, 665, 85
- Kennicutt, R. C., Jr. 1998, *ApJ*, 498, 541
- Kohandel, M., Pallottini, A., Ferrara, A., et al. 2019, *MNRAS*, 487, 3007
- Kroupa, P. 2001, *MNRAS*, 322, 231
- Krumholz, M. R., McKee, C. F., & Tumlinson, J. 2009, *ApJ*, 693, 216
- Laporte, N., Ellis, R. S., Boone, F., et al. 2017, *ApJL*, 837, L21
- Leitherer, C., Schaerer, D., Goldader, J. D., et al. 1999, *ApJS*, 123, 3
- Looser, T. J., D'Eugenio, F., Maiolino, R., et al. 2023, arXiv:2302.14155
- Mac Low, M.-M., & Ferrara, A. 1999, *ApJ*, 513, 142
- Maiolino, R., Scholtz, J., Wistok, J., et al. 2023, arXiv:2305.12492
- Mayer, L., Mastropietro, C., Wadsley, J., Stadel, J., & Moore, B. 2006, *MNRAS*, 369, 1021
- Pallottini, A., Ferrara, A., Bovino, S., et al. 2017a, *MNRAS*, 471, 4128
- Pallottini, A., Ferrara, A., Decataldo, D., et al. 2019, *MNRAS*, 487, 1689
- Pallottini, A., Ferrara, A., Gallerani, S., et al. 2017b, *MNRAS*, 465, 2540
- Pallottini, A., Ferrara, A., Gallerani, S., et al. 2022, *MNRAS*, 513, 5621
- Pallottini, A., Ferrara, A., Gallerani, S., Salvadori, S., & D'Odorico, V. 2014, *MNRAS*, 440, 2498
- Pereira-Wilson, M., Navarro, J. F., Benítez-Llambay, A., & Santos-Santos, I. 2023, *MNRAS*, 519, 1425
- Pérez-González, P. G., Barro, G., Annunziatella, M., et al. 2023, *ApJL*, 946, L16
- Planck Collaboration, Ade, P. A. R., Aghanim, N., et al. 2014, *A&A*, 571, A16
- Rosdahl, J., Blaizot, J., Aubert, D., Stranex, T., & Teyssier, R. 2013, *MNRAS*, 436, 2188
- Rosdahl, J., Schaye, J., Dubois, Y., Kimm, T., & Teyssier, R. 2017, *MNRAS*, 466, 11
- Salvadori, S., Ferrara, A., & Schneider, R. 2008, *MNRAS*, 386, 348
- Sobacchi, E., & Mesinger, A. 2013, *MNRAS*, 432, 3340
- Strait, V., Brammer, G., Muzzin, A., et al. 2023, *ApJL*, 949, L23
- Teyssier, R. 2002, *A&A*, 385, 337
- Vallini, L., Pallottini, A., Ferrara, A., et al. 2018, *MNRAS*, 473, 271
- Weingartner, J. C., & Draine, B. T. 2001, *ApJ*, 548, 296
- Wise, J. H., Abel, T., Turk, M. J., Norman, M. L., & Smith, B. D. 2012, *MNRAS*, 427, 311
- Ziparo, F., Ferrara, A., Sommovigo, L., & Kohandel, M. 2023, *MNRAS*, 520, 2445